Journal of the Korean Astronomical Society
55: 215 ∼ 220, 2022 December

https://doi.org/10.5303/JKAS.2022.55.6.215
pISSN: 1225-4614 · eISSN: 2288-890X
http://jkas.kas.org

Dynamic Formation and Associated Heating of a Magnetic Loop on the Sun

Tetsuya Magara[1,2], Yeonwoo Jang[2], and Donghui Son[2]

[1]Department of Astronomy and Space Science, Kyung Hee University, 1732, Deogyeong-daero, Giheung-gu, Yongin-si, Gyeonggi-do 17104, Republic of Korea
[2]School of Space Research, Kyung Hee University, 1732, Deogyeong-daero, Giheung-gu, Yongin-si, Gyeonggi-do 17104, Republic of Korea; magara@khu.ac.kr

Received November 3, 2022; accepted November 25, 2022

Abstract: To seek an atmospheric heating mechanism operating on the Sun we investigated a heating source generated by a downflow, both of which may arise in a magnetic loop dynamically formed on the Sun via flux emergence. Since an observation shows that the illumination of evolving magnetic loops under the dynamic formation occurs sporadically and intermittently, we performed a magnetohydrodynamic simulation of flux emergence to obtain a high-cadence simulated data, where temperature enhancement was identified at the footpoint of an evolving magnetic loop. Unlike a rigid magnetic loop with a confined flow in it, the evolving loop in a low plasma β atmosphere is subjected to local compression by the magnetic field surrounding the loop, which drives a strong supersonic downflow generating an effective footpoint heating source in it. This may introduce an energy conversion system to the magnetized atmosphere of the Sun, in which the free magnetic energy causing the compression via Lorentz force is converted to the flow energy, and eventually reduced to the thermal energy. Dynamic and thermodynamic states involved in the system are explained.

Key words: Sun: atmosphere — Sun: magnetic fields — magnetohydrodynamics — methods: numerical

1. Introduction

The Sun has a magnetized atmosphere extending toward the interplanetary space, where a number of magnetic loops coexist, as demonstrated by space missions such as Skylab, SMM, Yohkoh, SoHO, TRACE, Hinode, and SDO. Temperature in the atmosphere reaches a value more than hundred times higher than its surface value (Edlén 1942), and it is natural to consider a problem of identifying whether these loops contribute to enhancing the atmospheric temperature. They are mainly formed by a magnetic field emerging from the solar interior via the magnetic buoyancy (Parker 1955), so we may consider this problem in terms of the two distinct evolutionary phases of an emerging magnetic field: i) the early phase during which the magnetic field has emerged and is dynamically forming magnetic loops on the Sun; and ii) the late phase at which the formation of these loops has almost completed and they have well-developed magnetic structure.

When we focus on the late phase, a possible approach to the problem may be formulated in the following way: First, well-developed magnetic structure of a loop is given. Then, various types of perturbations are imposed on it. Finally, how these perturbations lead to enhancing the atmospheric temperature is investigated (Parker 1972; Heyvaerts & Schatzman 1980; Hollweg 1981; Sturrock & Uchida 1981; van Ballegooijen 1986; Parker 1988; Low 1990; Ofman et al. 1994; Inverarity & Priest 1995; Galsgaard & Nordlund 1996; Belien et al. 1999; Matthaeus et al. 1999; Cranmer & van Ballegooijen 2005; Aschwanden 2005; Kittinaradorn et al. 2009; Goossens et al. 2011; Reale 2014; Howson et al. 2019).

On the other hand, heating of a magnetic loop also occurs at the early phase, as found in observations. Figure 1 presents one such observation, showing that evolving loops were dynamically formed by a continuously emerging magnetic field. These loops were initially dark, some of which were then illuminated intermittently during their dynamic formation. This suggests that heating is associated with dynamic formation in the evolving loops which are fairly far from having well-developed magnetic structure. Interestingly, the successive panels 1b and 1c suggest that heating first occurred at one footpoint of an evolving loop, and the location of heating was then transferred upward along the loop.

What causes heating of those evolving loops under the dynamic formation? To answer this question, we need to investigate dynamic and thermodynamic processes involved in the emergence of magnetic flux from the solar interior (flux emergence, in short). Figure 1d schematically illustrates three key processes expected to occur through flux emergence. The 1st process is caused by the magnetic buoyancy; a loop filled with a dense plasma is lifted against the solar gravity by a downflow rarefying the plasma in the loop. The 2nd process occurs when the downflow collides with a low atmospheric layer with high density, which converts the flow energy to the thermal energy and generates a footpoint heating source. Heat is then transported upward

Corresponding author: T. Magara

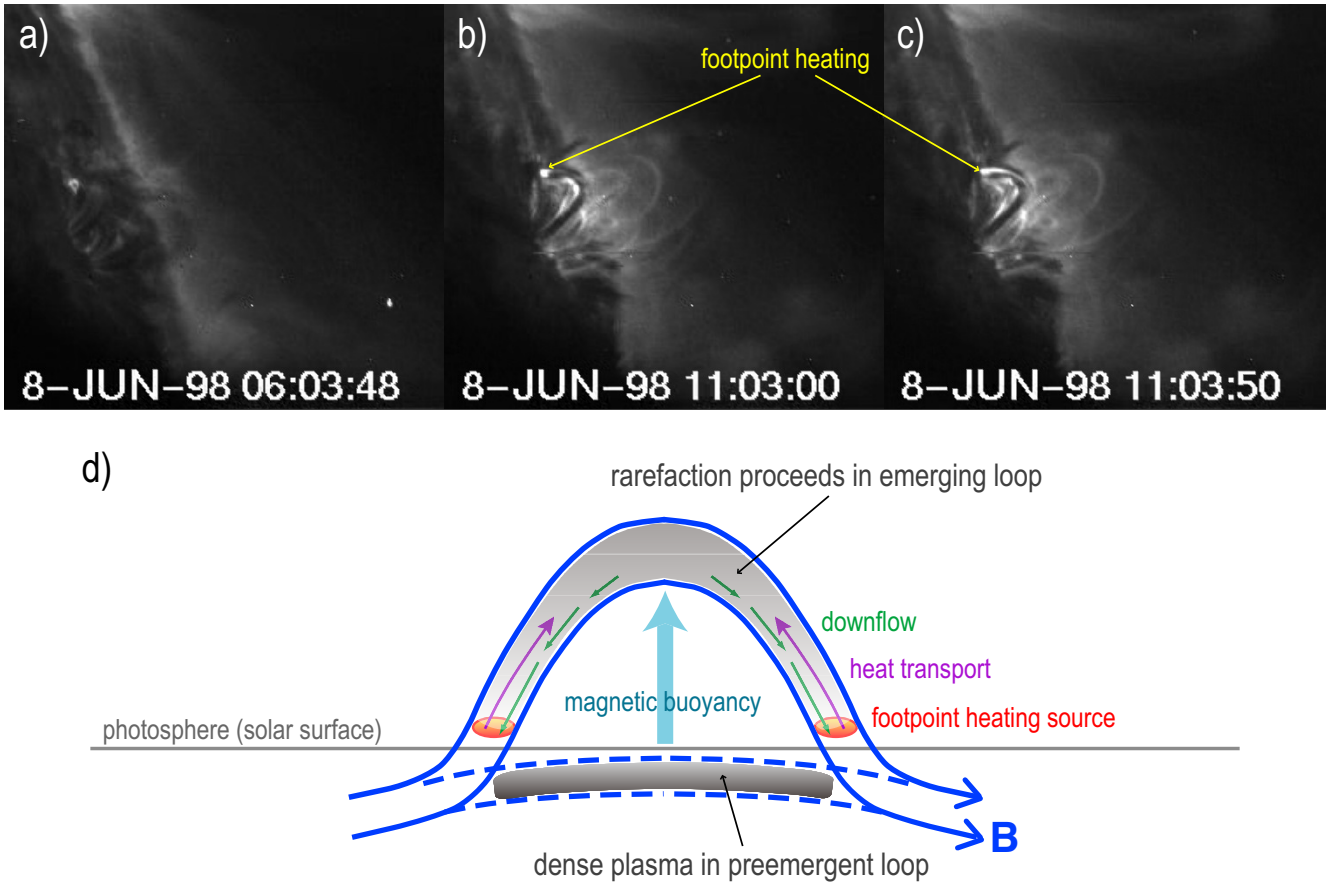

Figure 1. a–c: Formation of evolving magnetic loops via continuous emergence of magnetic field observed by TRACE. A possible footpoint heating location is indicated by the yellow arrow at panels b and c. A movie is provided (http://163.180.179.74/~magara/page31/Topics/CMEmodeling/trace171.2-11.mp4). d: Schematic illustration of flux emergence.

from the heating source, which is the 3rd process.

Here a central issue is the footpoint heating source generated by the downflow. It may not be effective at the late phase when the magnetic buoyancy with a strong downflow has almost terminated, although the early phase might be different because the buoyancy is surely active. It is beyond the scope of the present work to reproduce all the three processes, or rather, this letter reports an initial result of investigating the possibility that the downflow generates an effective footpoint heating source.

2. MODEL & RESULT

To investigate the central issue raised in the previous section, we used the magnetohydrodynamic (MHD) simulation of flux emergence reported in Magara (2017). Since the observation in Figure 1 shows that the illumination of the evolving loops occurred sporadically and intermittently, we reperformed the simulation to obtain a simulated data at five times higher cadence.

Figure 2 shows an evolving loop found in that data, at one footpoint of which temperature enhancement was identified. At the main panel of this figure, density distribution is displayed in a logarithmic scale using the color volume rendering, while distributions of temperature, divergence of flow velocity ($\nabla \cdot \mathbf{v}$, local compression/expansion rate), and vertical magnetic flux density are represented by the maps placed at $z = 6.6$ (green to pink color map), $y = 3.4$ (dark red to dark green color map), and $z = 0$ (grayscale map), respectively. Here a vertically upward direction is given by the z-axis and the photosphere (solar surface) is represented by the (x, y)-plane at $z = 0$. Normalization units are given by $2H_{ph}$ (length), c_{ph} (velocity), ρ_{ph} (gas density), $\rho_{ph}c_{ph}^2$ (gas pressure), T_{ph} (temperature), and $(\rho_{ph}c_{ph}^2)^{1/2}$ (magnetic field), where H_{ph}, c_{ph}, ρ_{ph}, and T_{ph} indicate the pressure scale height, adiabatic sound speed, gas density, and temperature at the photosphere. We adopted $\gamma = 5/3$ and $\mu = 0.6$ as the specific heat ratio and mean molecular weight, respectively, so $2H_{ph} = 540$ km in the simulation. A smaller panel is placed in the lower right corner of this figure, showing distributions of gas pressure (colors) and flow velocity (arrows) along part of the loop, in addition to the grayscale map of the photospheric magnetic flux density. The cross sectional area of the loop is represented by a field-line thickness.

The top panel in Figure 3 shows variations in loop height (black curve), field-aligned component of veloc-

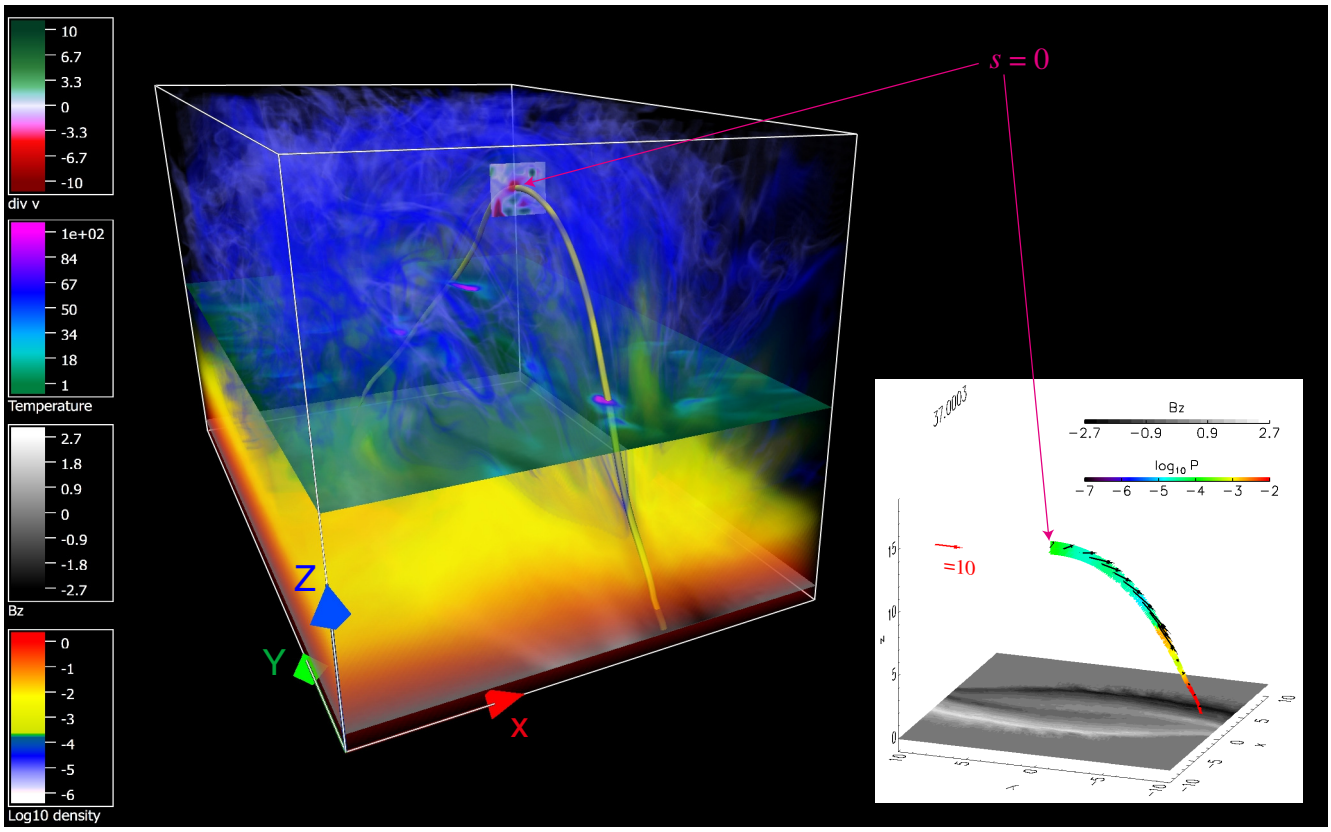

Figure 2. Main panel: Snapshot of an evolving magnetic loop (yellow field line) in MHD simulation of flux emergence. Density distribution is displayed in a logarithmic scale using color volume rendering, while distributions of temperature, $\nabla \cdot \mathbf{v}$, and vertical magnetic flux density are represented by maps placed at $z = 6.6$ (green to pink color map), $y = 3.4$ (dark red to dark green color map), and $z = 0$ (grayscale map), respectively. A vertically upward direction is given by the z-axis and the photosphere (solar surface) is represented by the (x, y)-plane at $z = 0$. Displayed domain size is $(-8, -9, -1) \leq (x, y, z) \leq (8, 17, 15)$. Length is normalized by 540 km. A movie is provided for a time period from $t = 30.2$ to $t = 40$ at a regular interval of 0.2 (http://163.180.179.74/~magara/Download/JKAS2022/fig2.mp4). Smaller panel in lower right corner: Distributions of gas pressure (colors) and flow velocity (arrows) along part of the loop are presented, in addition to the grayscale map of the photospheric magnetic flux density. The cross sectional area of the loop is represented by a field-line thickness, while the red arrow indicates a speed of 10 (normalized by photospheric sound speed). s in Figure 3 represents loop length measured from the same location indicated by the magenta arrows.

ity $v_{\parallel}$ (red curve), and Mach number based on that component of velocity $M_{\parallel}$ (blue curve) along the part of the loop displayed at the smaller panel of Figure 2, while variations in density (black curve), pressure (blue curve), and temperature (red curve) are presented in a logarithmic scale at the bottom panel. The areas colored yellow (I, III, V, VIII), green (II, IV, VI), and orange (VII) show selected regions where compression ($\nabla \cdot \mathbf{v} < 0$), expansion ($\nabla \cdot \mathbf{v} > 0$), and shock ($\nabla \cdot \mathbf{v} < 0$) occur, respectively. Here the front of the shock was determined by deriving the location where $\nabla \cdot \mathbf{v}$ changes the sign from positive to negative, which gives the upstream Mach number $M_{\parallel} = 4.3$ at this location. We then used it to calculate the downstream Mach number via Rankine-Hugoniot (RH) relation and derived a location with this downstream Mach number, which is the back of the shock. The temperature is reduced to 1 as the loop height is close to 0, which is caused by the radiative cooling term (Newton's law of cooling) incorporated to the energy equation of this simulation, given by

$$\mathsf{L}_{rad} = \rho C_v \frac{T - T_0(z)}{\tau_r} e^{-\left(\frac{z-z_0}{d}\right)^2}, \qquad (1)$$

where $z_0 \sim 1{,}000$ km and $d \sim 400$ km while $T_0(z)$ indicates the distribution of temperature prescribed according to a standard solar atmospheric model (Vernazza et al. 1981), $\tau_r \sim 1$ s (Stix 1991) is the radiative relaxation time, and C_v is the specific heat at constant volume.

3. Discussion

One of the prominent features of a magnetized atmosphere where the dynamic formation proceeds via flux emergence is that the atmosphere significantly deviates from a smoothly stratified state; that is, strongly compressed regions and strongly expanded regions highly mix there, as shown by the $\nabla \cdot \mathbf{v}$ map in Figure 2. In such a strongly compressed region a dense plasma will locally be produced (significant temperature enhancement is also expected there), which slides down

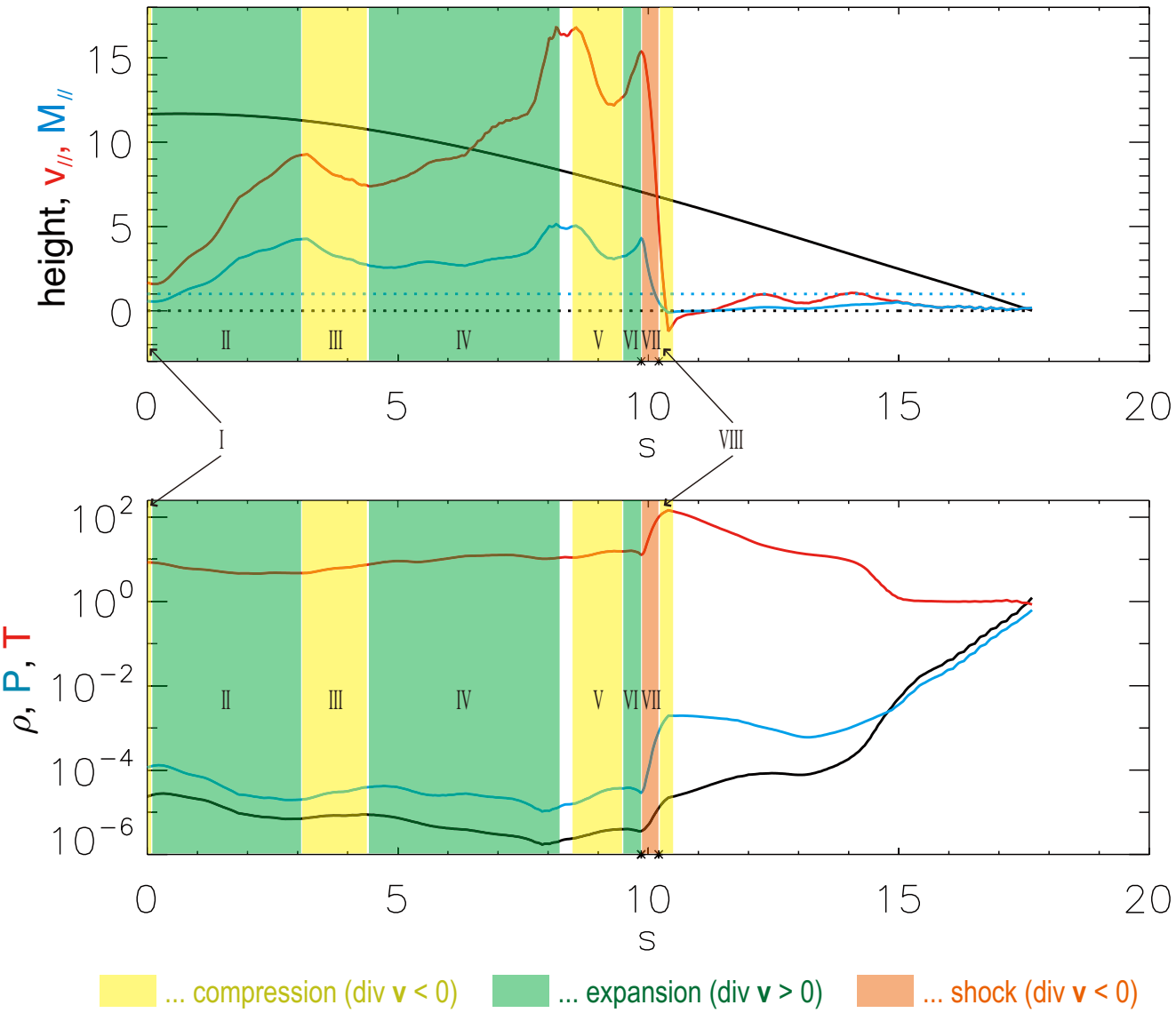

Figure 3. Top panel: Variations in loop height (black curve), field-aligned component of velocity $v_{\parallel}$ (red curve), and Mach number based on that component of velocity $M_{\parallel}$ (blue curve) along the part of the loop displayed at the smaller panel of Figure 2. The blue (black) dotted line indicates a level of 1 (0). Bottom panel: Variations in density (black curve), pressure (blue curve), and temperature (red curve). The areas colored yellow (I, III, V, VIII), green (II, IV, VI), and orange (VII) show selected regions where compression ($\nabla \cdot \mathbf{v} < 0$), expansion ($\nabla \cdot \mathbf{v} > 0$), and shock ($\nabla \cdot \mathbf{v} < 0$) occur, respectively. The asterisks indicate the front and back of the shock. s represents loop length measured from the same location indicated by the magenta arrows in Figure 2.

along a magnetic loop, thereby forming elongated high-density structure in the atmosphere. This gives rise to the blue multiple loop-like structure of density in Figure 2 (see also http://163.180.179.74/~magara/Download/JKAS2022/fig2.mp4).

Another prominent feature is found in dynamic and thermodynamic states inside the evolving loop explained by Figure 3. Compared to the schematic illustration in Figure 1d, where a smooth downflow exists, Figure 3 reveals that compressed regions and expanded regions are alternately distributed along the loop. Note that unlike a confined flow in a rigid loop, the variations in Figure 3 do not give the evolutionary path of a downflowing plasma, or rather, the figure shows a snapshot of the dynamic and thermodynamic states of the plasma inside the evolving loop taken at a certain time. During an expansion phase of the plasma, its downflow tends to be accelerated by gas pressure gradient force as well as gravitational force along the loop. Figure 3 shows that the downflow reaches a speed well above the free-fall speed $(2\, g_0\, \Delta h)^{1/2} = 3.3$ with $g_0 = 1.2$ and $\Delta h = 4.6$, at the front of the shock. The shock produces a temperature enhancement of 8 (this is 1.2 times larger than the value obtained by RH relation with the assumption that the downflow has only a field-aligned component of velocity whose upstream Mach number is $M_{\parallel} = 4.3$).

Further compression of the plasma and deceleration of the downflow are found behind the shock, and all flow energy is converted to the thermal energy in Region VIII under that assumption (i.e., $M_{\parallel} = 0$). The temperature reaches a value more than 100 in this region which may correspond to the transition region of the Sun.

For such an evolving magnetic loop in a low plasma β atmosphere as discussed here, a downflowing plasma in it could be compressed by the magnetic field surrounding the loop, which may drive a strong supersonic downflow generating an effective footpoint heating source in it. This leads us to expect that an energy conversion system is introduced to the magnetized atmosphere of the Sun, in which the free magnetic energy causing the compression via Lorentz force is converted to the thermal energy.

Two comments are made before closing our report. One of them is on the property of a magnetic loop where an effective footpoint heating source is generated. According to the blue multiple loop-like structure of density explained above, we expect that a number of high-density loops are formed in the atmosphere, although the temperature map in Figure 2 suggests that only selected loops have effective footpoint heating sources. This means that a loop with an effective footpoint heating source has a characteristic property based on dynamic and thermodynamic states inside it. We will investigate these states inside various loops obtained from the MHD simulation and try to identify the characteristic property.

The other comment is on the third process mentioned in introduction, by which heat is transported upward from an effective footpoint heating source. Obviously the present work just shows the generation of an effective footpoint heating source, which is in fact an initial process toward the formation of an illuminated loop shown by the observation in Figure 1. To demonstrate the succeeding process, we may have to perform a separate simulation where thermal conduction is included, which will be treated in our forthcoming paper.

Acknowledgments

T.M. deeply appreciates the referee's useful comments on the paper. The authors wish to thank the Kyung Hee University for general support of this work. Part of Figure 1 was made using images obtained by the Transition Region and Coronal Explorer (TRACE). TRACE is a mission of the Stanford-Lockheed Institute for Space Research, and part of the NASA Small Explorer program. The main panel of Figure 2 was made using VAPOR (Clyne et al. 2007). This work was financially supported by a research program (NRF-2021R1A2C1010310, PI: T. Magara) through the National Research Foundation of Korea (NRF) funded by the Ministry of Education, Science and Technology.

References

Aschwanden, M. J. 2005, Physics of the Solar Corona. An Introduction with Problems and Solutions (2nd edition), Praxis Publishing Ltd., Chichester, UK, Springer, New York, Berlin

Belien, A. J. C., Martens, P. C. H., & Keppens, R. 1999, The Dynamical Influence Of The Transition Region And Chromosphere On The Heating Of Coronal Loops By Resonant Absorption Of Alfvén Waves, 8th SOHO Workshop: Plasma Dynamics and Diagnostics in the Solar Transition Region and Corona, 446, 167

Clyne, J., Mininni, P., Norton, A., & Rast, M. 2007, Interactive desktop analysis of high resolution simulations: application to turbulent plume dynamics and current sheet formation, New J. Phys., 9, 301

Cranmer, S. R., & van Ballegooijen, A. A. 2005, On the Generation, Propagation, and Reflection of Alfvén Waves from the Solar Photosphere to the Distant Heliosphere, ApJS, 156, 265

Edlén, B. 1942, Die Deutung der Emissionslinien im Spektrum der Sonnenkorona, Z. Astrophys., 22, 30

Galsgaard, K., & Nordlund, Å. 1996, Heating and activity of the solar corona 1. Boundary shearing of an initially homogeneous magnetic field, JGR, 101, 13445

Goossens, M., Erdélyi, R., & Ruderman, M. S. 2011, Resonant MHD Waves in the Solar Atmosphere, SSRv, 158, 289

Heyvaerts, J., & Schatzman, E. 1980, Electro Magnetic Heating of Coronae, Japan-France Seminar on Solar Physics, 77

Hollweg, J. V. 1981, Alfvén waves in the solar atmosphere, SoPh, 70, 25

Howson, T. A., De Moortel, I., Reid, J., et al. 2019, Magnetohydrodynamic waves in braided magnetic fields, A&A, 629, A60

Inverarity, G. W., & Priest, E. R. 1995, Turbulent coronal heating. III. Wave heating in coronal loops, A&A, 302, 567

Kittinaradorn, R., Ruffolo, D., & Matthaeus, W. H. 2009, Solar Moss Patterns: Heating of Coronal Loops by Turbulence and Magnetic Connection to the Footpoints, ApJL, 702, L138

Low, B. C. 1990, Equilibrium and dynamics of coronal magnetic fields, ARA&A, 28, 491

Magara, T. 2017, Structural properties of the solar flare-producing coronal current system developed in an emerging magnetic flux tube, PASJ, 69, 5

Matthaeus, W. H., Zank, G. P., Oughton, S., et al. 1999, Coronal Heating by Magnetohydrodynamic Turbulence Driven by Reflected Low-Frequency Waves, ApJ, 523, L93

Ofman, L., Davila, J. M., & Steinolfson, R. S. 1994, Coronal Heating by the Resonant Absorption of Alfven Waves: The Effect of Viscous Stress Tensor, ApJ, 421, 360

Parker, E. N. 1955, The Formation of Sunspots from the Solar Toroidal Field, ApJ, 121, 491

Parker, E. N. 1972, Topological Dissipation and the Small-Scale Fields in Turbulent Gases, ApJ, 174, 499

Parker, E. N. 1988, The origins of the stellar corona, Solar and Stellar Coronal Structure and Dynamics, 2

Reale, F. 2014, Coronal Loops: Observations and Modeling of Confined Plasma, Living Rev. Sol. Phys., 11, 4

Stix, M. 1991. The Sun. an Introduction, Springer-Verlag Berlin Heidelberg New York

Sturrock, P. A., & Uchida, Y. 1981, Coronal heating by stochastic magnetic pumping, ApJ, 246, 331

van Ballegooijen, A. A. 1986, Cascade of Magnetic Energy as a Mechanism of Coronal Heating, ApJ, 311, 1001

Vernazza, J. E., Avrett, E. H., & Loeser, R. 1981, Structure of the solar chromosphere. III. Models of the EUV brightness components of the quiet sun., ApJ, 45, 635